Velocity Measurements in 3-D Cavity Flows by PIV(Particle Imaging Velocimetry)

*Young-Ho Lee**

입자영상속도계에 의한 3차원 캐비티 유동의 속도계측

이 영 호

Abstract

Particle Imaging Velocimetry(PIV) was adopted to measure velocities in a lid-driven three-dimensional cavity flow. A comparison with experimental results by LDA was made and good agreement was confirmed. The reliability of the present method was validated further by systematic uncertainty analyses.

Flow characteristics associated with the cavity flow were discussed in terms of spanwise aspect ratios of 1 : 1 and 1 : 3.2 and four Reynolds numbers of 10^3, 3.2×10^3, 5×10^3 and 10^4. The existence of spanwise symmetric flow patterns is characterized.

Introduction

LDA(Laser Doppler Anemometer) is regarded as one of the useful means to analyse the unsteady flow of high frequency fluctuations. But, practically, it compasses an inevitable demerit of finite fixed measuring points and inability to obtain separate velocity data instantaneously. The recent advent of less expensive, high performance computer, on the other hand, has enhanced the availability of digital image processing methods for the quantitatively satisfactory comprehension of flow fields. Consequently, PIV(Particle Imaging Velocimetry) has become an efficient method to acquire simultaneous multi-point velocity data, supported by reliable processing algorithms.

* 본 논문은 제2회 한일유체공학 심포지움(1990년 10월, 서울)에서 강연한 내용임.

* Dept. of Marine Engineering, Korea Maritime Univ.

As an experimental example, 3-dimensional lid-driven cavity flows were investigated. The cavity flow, abundant in complex flow properties has been quoted frequently as a bench-mark problem by numerical investigators[1], mainly due to its simple boundary conditions. Recently, experimental results were reported by means of the visualization method and LDA[2)~3)]. But they were discussed in the limited parts of the flow field and more reasonable analyses of the existing errors were also required.

PIV of the present study reveals satisfactory agreements with the previous results by LDA and experimental data are also further validated by the uncertainty analysis suggested by ANSI/ ASME[4].

Two kinds of aspect ratio of 1 : 1 and 1 : 3.2 are adopted and four cases of Reynolds number of 10^3, 3.2×10^3, 5×10^3 and 10^4 are selected for the individual aspect ratio.

General Descriptions of PIV

A schematic arrangement of the experimental apparatus is shown in Fig. 1. A continuously moving stainless belt of 0.25mm T×160mm B×1462mm L supplies lid-driven shear force in the cavity. Spherical particles of nylon12, ranging from 0.12 to 0.25mm in diameters are selected as tracer particles. Lighting system consisting of an argon laser generator, flexible fiber cables and a cylindrical lens attached to a 3-axis traverser yield sheet light of constant thickness of 2.5mm. Pictures of the flow field are recorded on commercial video-tapes, which supply, afterwards, separate 4 consecutive frames of dispersed particles image and they are transformed into digitized informations expressed in particle size and position through the digital image processor. A flow chart of the data processing adopted in the present method is presented in Fig. 2. Up to the calculation of gravity centers, data are pre-processed on the image processor.

What is important in post processing is "identification", a tracking technique of the same particle on the consecutive 4 frames of pictures. An identification method free from excessive errors was established by T.Kobayashi et al.[5] and adopted here for the average numbers of 500 -800 particles in one processing case. Time intervals from the 1st to 4th frame ranging from 0.5sec to 3.0sec are decided on the real flow conditions.

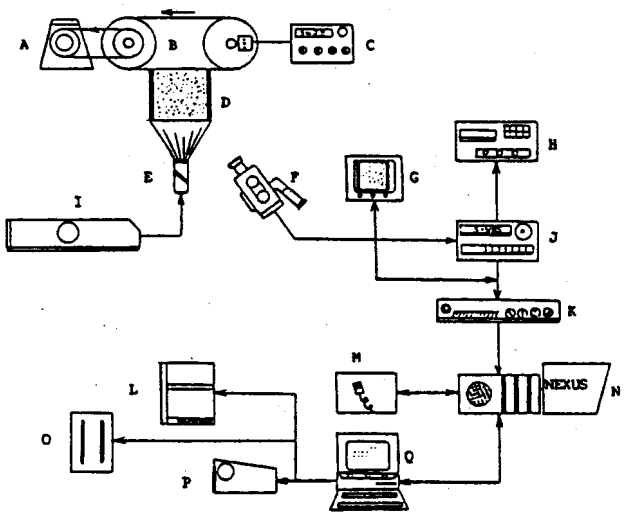

A:SCR DC Motor & Reduction Gear
B:Roller & Stainless Belt
C:Encoder & Digital Tachometer
D:Cavity(100 mm L,B,H)
E:Cylindrical Lens & Fiber Line
F:TV Camera or CCD Camera
G:Monitor TV
H:Color Image Printer
I:Argon Laser
J:Video Tape Recorder
K:Time Base Corrector
L:X-Y Plotter
M:Digitizer
N:Image Processor & Monitor
O:External Memory
P:Laser Printer
Q:Host Computer

Fig. 1 Schematic Experimental Apparatus

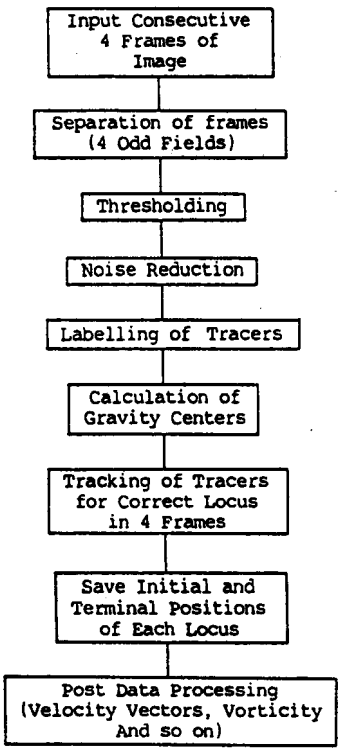

Fig. 2 Flow Chart of Digital Image Processing

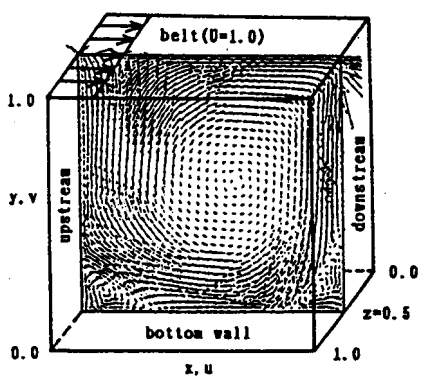

Fig. 3 Schematic Definition of Coordinates

Uncertainty Analysis

Quantitative measurements of velocity informations by way of the particle tracking method always accompany finite measuring errors. Recently Yamamoto et al.[6] suggested their estimation

of errors or uncertainty, occurring in velocity measurements. Here is summarized an uncertainty analysis of the velocity data, according to the descriptions of the ANSI/ASME.

As an example, the case of SAR=1 : 1, $Re=3.2\times10^3$ is discussed for the representative velocity $0.5U_B$ (U_B is belt speed). Dimensionless velocity is calculated from the following equation.

$$U^*=\frac{H\times P_{41}\times 10^4}{L\times s\times n\times dt}$$

Here, H =length of cavity=100mm

P_{41} =pixel numbers corresponding to $0.5U_B$=60 pixels

L =length of cavity in pixel numbers=400 pixels

s =peripheral length of rubber roller=617mm

n =pulse number on tachometer=488.3pulse at 20°C

dt =time interval on 4 frames=1.0sec

The absolute bias limit and precision limit are combined by the root-sum square (RSS) calculation for the various error components numbering 21 elementary sources.

item	bias limit	precision limit
H	0.112mm	0.0
P_{41}	2.07pixel	1.16pixel
L	2.0pixel	0.0
s	0.5mm	0.0
n	3.65pulse	0.0
dt	0.0sec	0.0

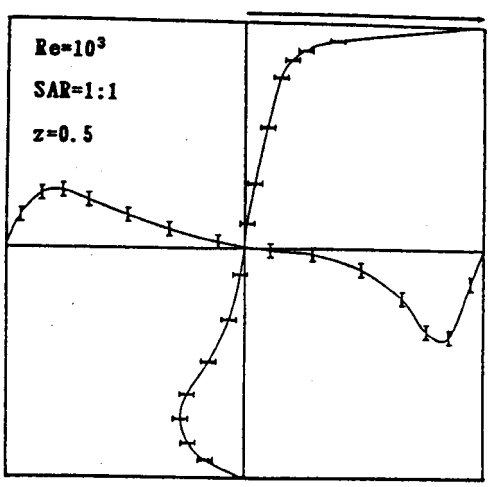

Fig. 4 Relative RSS Uncertainty for SAR=1 : 1, $Re=10^3$

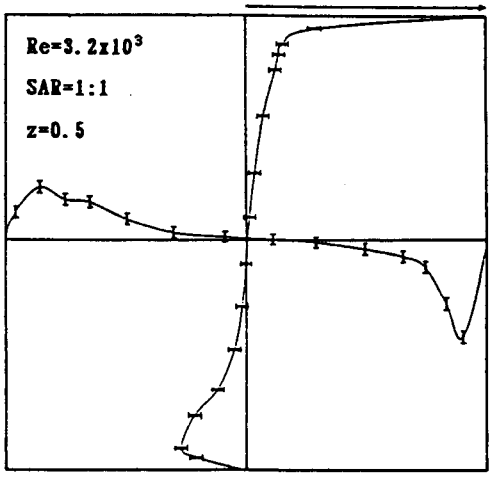

Fig. 5 Relative RSS Uncertainty for SAR=1 : 1, Re=3.2×10^3

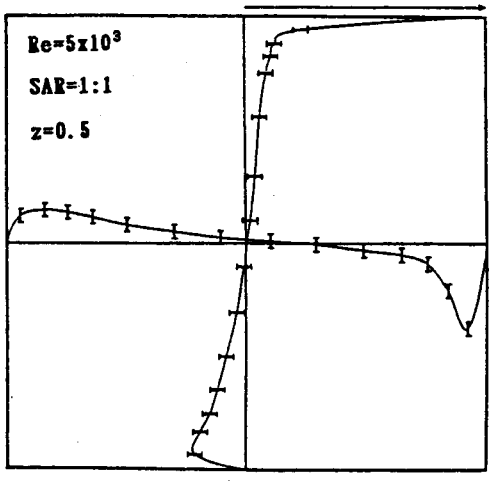

Fig. 6 Relative RSS Uncertainty for SAR=1 : 1, Re=5×10^3

The relative bias limit and precision limit are also given as follows.

item	bias limit	precision limit
H	0.112/100=0.0	0.0
P_{41}	2.07/60=0.03	1.16/60=0.018
L	2/400=0.005	0.0
s	0.5/617=0.00081	0.0
n	3.65/488=0.0075	0.0
dt	0.0/1.0=0.0	0.0

The final report on the uncertainty is summarized in two separate forms.

Absolute Uncertainty

representative velocity=0.5(D-less)

bias error B_{ABS} =0.0166

precision error S_{ABS} =0.009, $\nu>30$

$U_{ABS,ADD}$=0.0347(about 99% coverage)

$U_{ABS,RSS}$=0.0246(about 95% coverage)

Relative Uncertainty

representative velocity=0.5(D-less)

bias error B_{REL} =0.033

precision error S_{REL} $=0.018$, $\nu>30$

$U_{REL,ADD}=0.069=6.9\%$ (about 99% coverage)

$U_{REL,RSS}=0.049=4.9\%$ (about 95% coverage)

Same procedures cited in the preceding contents are iterated for different velocity components and Reynolds numbers. Approximate equations of $U_{REL,RSS}$ are formulated for SAR=1 : 1 as follows.

$$Re=10^3,\ U_{REL,RSS}(\%)=e^{(-0.9686\times\log U-2.9028)}\times 100(\%)$$

$$Re=3.2\times10^3,\ U_{REL,RSS}(\%)=e^{(-0.9809\times\log U-3.658)}\times 100(\%)$$

$$Re=5\times10^3,\ U_{REL,RSS}(\%)=e^{(-0.9936\times\log U-3.4580)}\times 100(\%)$$

Graphic representations by applying the above equations into velocity profiles at the central section $z=0.5$ are exhibited in Fig. 4, Fig.5 and Fig.6.

Experimental Results and Discussion

A schematic definition of coordinates is shown in Fig.3. Section of $z=0.5$ is usually selected as a typical flow field for discussions.

In Fig.7 and Fig.8, results by LDA measurement[3] are compared with those of the present method. Fairly good agreement is found, which confirms sufficiently that PIV may be regarded as a compatible measuring method against the LDA, enjoying merit of simultaneous multi-point measurements. Undesirably sacrificed unsteady analysis in the present study may not be open to criticisms because it is mainly owing to the lack of memory capacity on image processor.

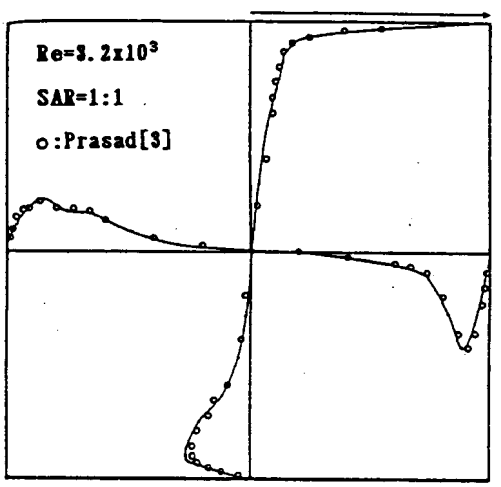

Fig. 7 Comparison with LDA Results for SAR=1 : 1, $Re=3.2\times10^3$

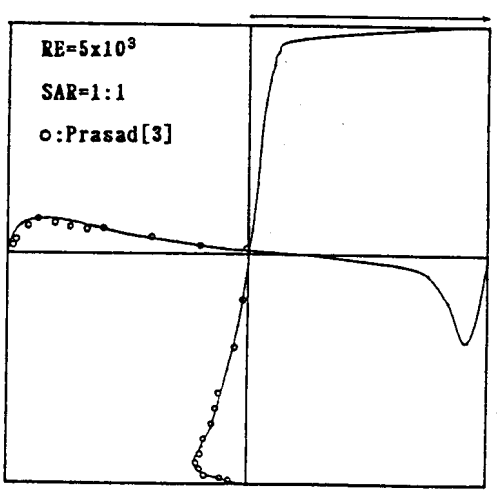

Fig. 8 Comparisons with LDA Results for SAR=1 : 1, $Re=5\times10^3$

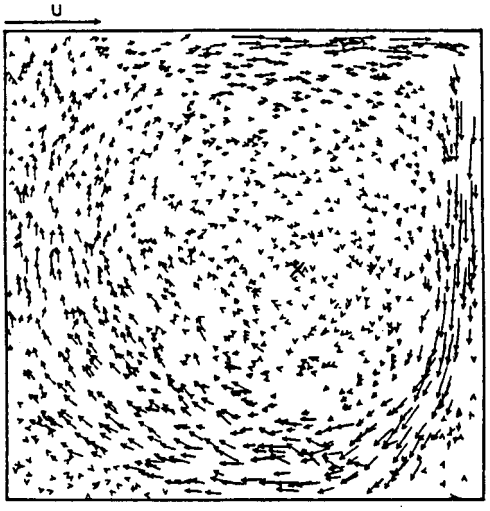

Fig. 9 Velocity Distributions at $z=0.5$ for SAR=1 : 1, Re=5×10^3

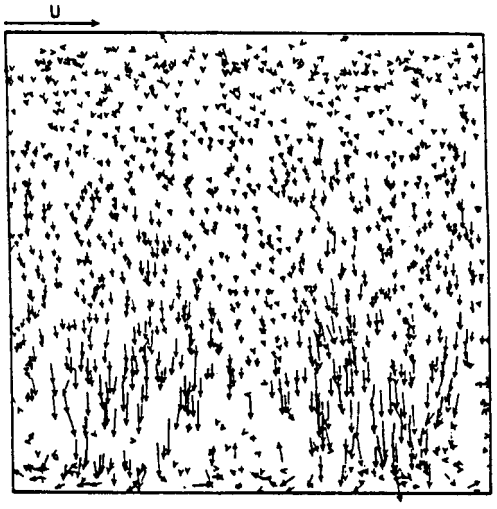

Fig. 10 Velocity Distributions at $x=0.9$ for SAR=1 : 1, Re=5×10^3

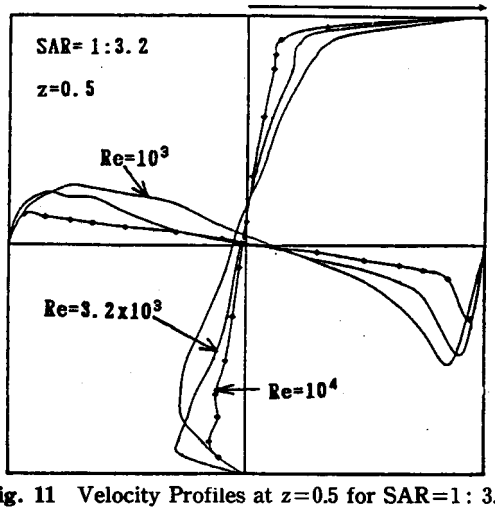

Fig. 11 Velocity Profiles at $z=0.5$ for SAR=1 : 3.2

Velocity vectors for SAR=1 : 1, Re=5×10^3 are distributed in Fig.9 and Fig.10. Total numbers of dispersed particles are ranging up to about 2000. Final data are overlapped summation of the consecutive 15 separate frames data processed continuously with the same time increment 40 sec.

Spatially-mean, spline curve-fitted velocity profiles in the range of $x=0.5\pm0.1$ and $y=0.5\pm0.1$ in case of SAR=1 : 3.2 are also presented in Fig.11. Velocity dispersions in case of SAR=1 : 1, Re=10^3 and SAR=1 : 3.2, Re=10^4 at the same region are shown by the symbolized marks in Fig. 12 and Fig.13 respectively.

Figure 14 and Fig.15 represent instantaneous streaklines by the dispersed particles for SAR=1 : 1, Re=5×10^3, section of $z=0.5$ spanwise center and x=0.9, 10mm apart from the downstream wall. Two corner vortices and single pair of TGL vortices are found near the bottom wall.

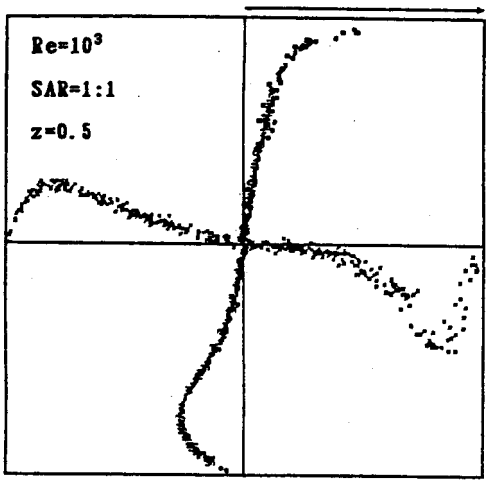

Fig. 12 Velocity vector Dispersions at $z=0.5$ for SAR=1 : 1, Re=10^3

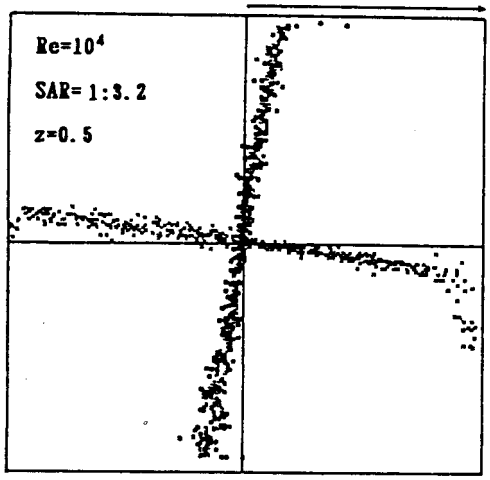

Fig. 13 Velocity vector Dispersions at $z=0.5$ for SAR=1 : 3.2, Re=10^4

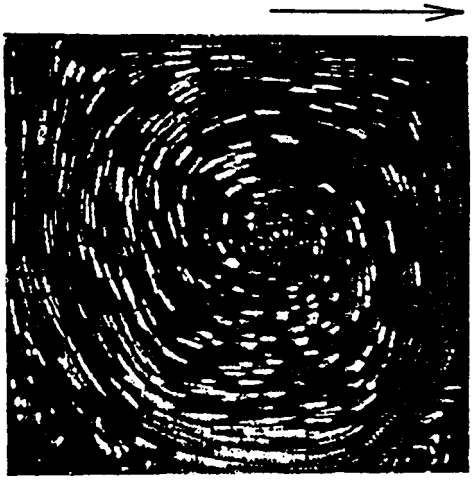

Fig. 14 Instantaneous Particle Streaklines for SAR=1 :1, Re=5×10^3, $z=0.5$

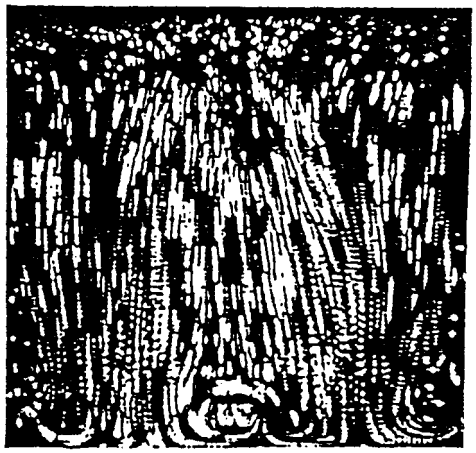

Fig. 15 Instantaneous Particle Streaklines for SAR=1 : 1, Re=10^3, x=0.9

In Fig.16 and Fig.17, good symmetry is maintained for the relatively high Reynolds number of 5×10^3 of SAR=1 : 1 and supposedly also for Re=10^4 of SAR=1 : 3.2 because there are found even dispersion of symbols and velocity profile similar to a forced vortex appearing in Fig.13.

Figure18 shows spanwise distributions of kinetic energy in four specific sections of SAR=1 : 1, Re=5×10^3. Generally good symmetries exist centering on $z=0.5$ section. A pair of kinetic energy

peaks are found at x=0.8, 20mm apart from the downstream wall but adverse distribution is followed at y=0.2, 20mm upward from the bottom wall. Uniform distributions at upstream wall of x=0.2, by the fully-developed TGL vortices and below the moving belt of y=0.8 by strong shear stress are also observed.

Consequently, global re-circulating variations of kinetic energy are characterized by the symmetric adverse peaks along the downstream to bottom wall and uniform distributions along the upstream wall to strong shear-governed region.

Any noise components existing in the present experiments, for example, minor leak from or into cavity, convective flow by small temperature variation, motor revolution fluctuation, two-phase flow characteristics and initial asymmetric flow pattern are not assumed to become decisive perturbations to cause bi-stable or complete random flow behaviors in terms of the time-mean characteristics for the all flow conditions considered in the present study.

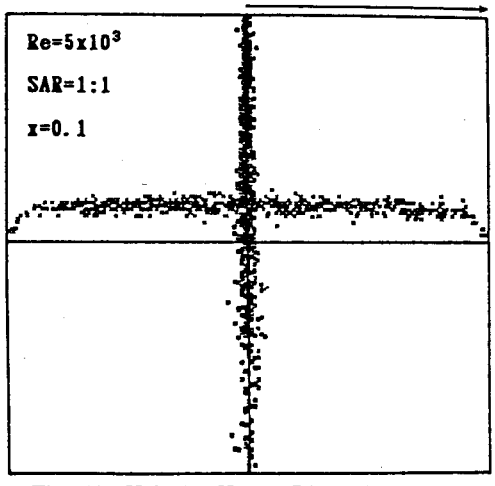

Fig. 16 Velocity Vector Dispersions at x=0.1 for SAR=1 : 1, Re=5×10³

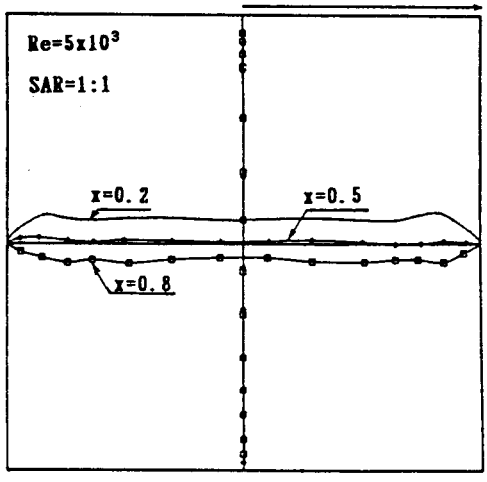

Fig. 17 Velocity Profiles at 3 x-sections for SAR=1 : 1, Re=5×10³

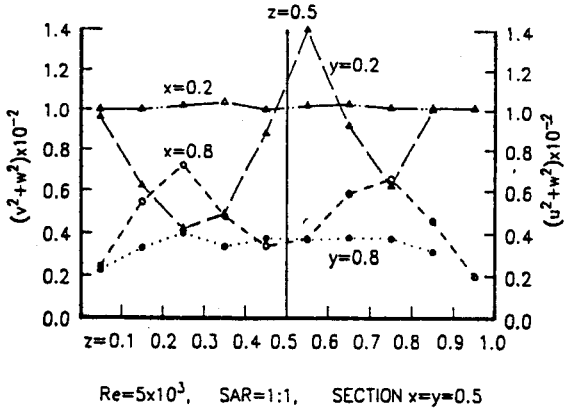

Fig. 18 Spanwise Distributions of Apparent Kinetic Energy for SAR=1 : 1, Re=5×10³

Conclusion

1. A quantitative comparison of the experimental results with those of LDA for a 3-dimensional lid-driven cavity flow reveals satisfactory agreements and ascertains the reliability of PIV (Particle Imaging Velocimetry) as an effective method deserving additional merits of simultaneous multi-point data acquisitions.

2. Uncertainty analysis for six parameters including twenty-one error sources yield, as typical uncertainties of $0.5U_B$ (U_B is belt speed), 10.6%, 4.9% and 6.2% relative RSS uncertainties for $Re=10^3$, 3.2×10^3 and 5×10^3 of SAR=1 : 1 respectively.

3. Time-mean spanwise symmetry of velocity profiles for $Re=5\times10^3$ of SAR=1 : 1 is obtained and supposedly also for the case of $Re=10^4$ of SAR=1 :3.2 because there exist even dispersions of velocity vector at $z=0.5$ section and also velocity profile similar to a forced vortex.

4. Spanwise distributions of apparent kinetic energy at four 90 degree rotating sections in case of $Re=5\times10^3$ of SAR=1 : 1, exhibit symmetric adverse peaks along the downstream to bottom wall, and uniform distributions along the upstream to shear-driven regions.

References

1) C.J. Freitas, R.L. Street, Non-linear Transient Phenomena in a Complex Recirculating Flow : A Numerical Investigation, Int. J. for Numerical Methods in Fluids, Vol. 8, 1988, p. 769.
2) A.K. Prasad, C.Y. Perng, J.R. Koseff, Some Observations on the Influence of Longitudinal Vortices in a Lid-Diven Cavity Flow, AIAA CP-3654, 1988, p. 288.
3) A.K. Prasad, J.R. Koseff, Reynolds Number and End-wall Effects on a Lid-Driven Cavity Flow, Phys. Fluids A Vol. 1(2), Feb. 1989, p. 208.
4) ANSI/ASME PTC19.1-1985, Measurement Uncertainty, Suppl. PTC(1986), ASME.
5) T. Kobayashi, T. Saga, K. Sekimoto, Velocity Measurement of Three-Dimensional Flow around Rotating Parallel Disks by Digital Image Processing, Flow Visualization -1989, ASME FED Vol. 85, 1989, p. 29.
6) F. Yamamoto, Y. Dai, M. Koukawa, M. Itoj, T. Uemura, Numerical Simulation of Error Analysis in Particle Tracking Velocimeter by Correlation Method, Flow Visualization-1989, ASME FED Vol. 85, 1989, p. 9.